ACS Infectious Diseases

pubs.acs.org/journal/aidcbc

Letter

Recognition of Divergent Viral Substrates by the SARS-CoV-2 Main Protease

Elizabeth A. MacDonald, Gary Frey, Mark N. Namchuk, Stephen C. Harrison, Stephen M. Hinshaw,* and Ian W. Windsor*

Cite This: https://doi.org/10.1021/acsinfecdis.1c00237

Read Online

ACCESS | Metrics & More | Article Recommendations | Supporting Information

ABSTRACT: The main protease (M^{pro}) of severe acute respiratory syndrome coronavirus 2 (SARS-CoV-2), the cause of coronavirus disease (COVID-19), is an ideal target for pharmaceutical inhibition. M^{pro} is conserved among coronaviruses and distinct from human proteases. Viral replication depends on the cleavage of the viral polyprotein at multiple sites. We present crystal structures of SARS-CoV-2 M^{pro} bound to two viral substrate peptides. The structures show how M^{pro} recognizes distinct substrates and how subtle changes in substrate accommodation can drive large changes in catalytic efficiency. One peptide, constituting the junction between viral nonstructural proteins 8 and 9 (nsp8/9), has P1′ and P2′ residues that are unique among the SARS-CoV-2 M^{pro} cleavage sites but conserved among homologous junctions in coronaviruses. M^{pro} cleaves nsp8/9 inefficiently, and amino acid substitutions at P1′ or P2′ can enhance catalysis. Visualization of M^{pro} with intact substrates provides new templates for antiviral drug design and suggests that the coronavirus lifecycle selects for finely tuned substrate-dependent catalytic parameters.

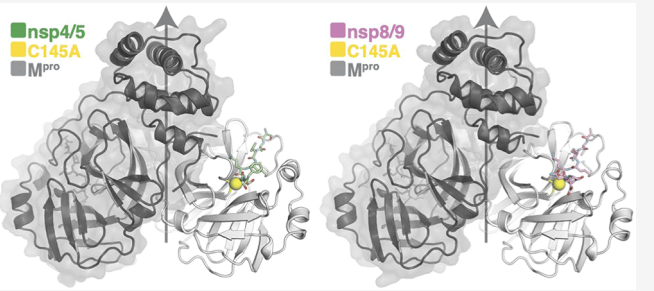

KEYWORDS: *SARS-CoV-2, M^{pro}, protease, virology*

The development and stockpiling of pan-coronavirus antiviral drugs for pandemic prevention has been a goal since the SARS outbreak of 2003.[1,2] The coronavirus main protease (nsp5 or M^{pro}, where nsp is nonstructural protein) is a conserved drug target and a focus of these efforts. Hundreds of M^{pro} inhibitors have been reported. Most of these drugs occupy the active site cleft responsible for recognizing the N-terminal fragments of substrate peptides, and many form covalent bonds to the active site cysteine of M^{pro} (Cys145).[3−7] A recent crystal structure of the nsp5/6 acyl-enzyme intermediate provides one template for chemical mimicry of this essential catalytic step.[8] We provide evidence that enzyme−substrate contacts on both sides of the M^{pro} catalytic site affect the rate of formation of the covalent complex, a characteristic that could be exploited by new protease inhibitors.

The nsp8/9 junction is a conserved M^{pro} substrate (Figure 1A,B). The nearly invariant Asn residues at P1′ and P2′ are unique within a given coronavirus polyprotein; Gly, Ser, or Ala predominate at these positions in the other substrates.[9] The cleavage of nsp8/9 is slow but required for replication of the closely related Murine Hepatitis Virus.[10] Indeed, a recently determined cryo-EM structure shows that the N-terminus of nsp9 contacts nsp12, a core component of the viral RNA polymerase.[11] In this context, the nsp8/9 P1′ to P3′ residues contribute to a binding site for a nucleotide that is transferred to the amino terminus of the P1′ residue.[12] Therefore, the nsp8/9 junction has evolved to satisfy two evolutionary constraints required for viral replication: it must be cleaved in the M^{pro} active site, and it must serve as a substrate in a nucleotide monophosphate transfer reaction catalyzed by

A

```
nsp4/5: TSAVLQ/SGFRKM
nsp5/6: SGVTFQ/SAVKRT
nsp6/7: KVATVQ/SKMSDV
nsp7/8: NRATLQ/AIASEF
nsp8/9: SAVKLQ/NNELSP
nsp9/10: ATVRLQ/AGNATE
nsp10/12: REPMLQ/SADAQS
nsp12/13: PHTVLQ/AVGACV
nsp13/14: NVATLQ/AENVTG
nsp14/15: TFTRLQ/SLENVA
nsp15/16: FYPKLQ/SSQAWQ
```

B

```
                nsp8/nsp9
SARS-CoV2: SAVKLQ/NNELSP
SARS-CoV: SAVKLQ/NNELSP
MERS: SAVKLQ/NNEIKP
OC43: SATVLQ/NNELMP
HKU1: ANAVMQ/NNELMP
229E: RVVKLQ/NNEIMP
NL63: RVVKLQ/NNEIMP
P6...P1/P1′..P6′
```

Figure 1. Viral M^{pro} substrates. (A) Protein sequence alignment of the 11 SARS-CoV-2 M^{pro} cleavage sites required for maturation of SARS-CoV2. (B) Protein sequence alignment of nsp8/9 M^{pro} cleavage sites from representative coronaviruses.

Received: April 28, 2021

Table 1. Catalytic Efficiencies for M^{pro} Substrates and Analogs

substrate	sequence[a]	k_{cat} (s^{-1})	K_M (μM)	k_{cat}/K_M (M^{-1} s^{-1})	fold change[b]
nsp4/5	TSAVLQ/SGFRKM	0.52 ± 0.07	41 ± 9	1.3 ± 0.3 × 10^4	
nsp8/9	RVVKLQ/NNELMP	0.013 ± 0.001	36 ± 6	3.6 ± 0.7 × 10^2	1.0
nsp8/9 N1′A	RVVKLQ/ANELMP	0.022 ± 0.001	22 ± 3	1.0 ± 0.1 × 10^3	2.9
nsp8/9 N2′A	RVVKLQ/NAELMP	0.034 ± 0.002	46 ± 5	7.5 ± 0.8 × 10^2	2.1
nsp8/9 N1′D	RVVKLQ/DNELMP				
nsp8/9 N2′D	RVVKLQ/NDELMP	0.0029 ± 0.0001	19 ± 1	1.6 ± 1.2 × 10^2	0.4

[a]Lys-DABCYL and Glu-EDANS are appended to the N- and C-termini. Residues that differ from the wild-type sequence are bolded. [b]Fold change = $(k_{cat}/K_M)_{nsp8/9\ analog}/(k_{cat}/K_M)_{nsp8/9}$.

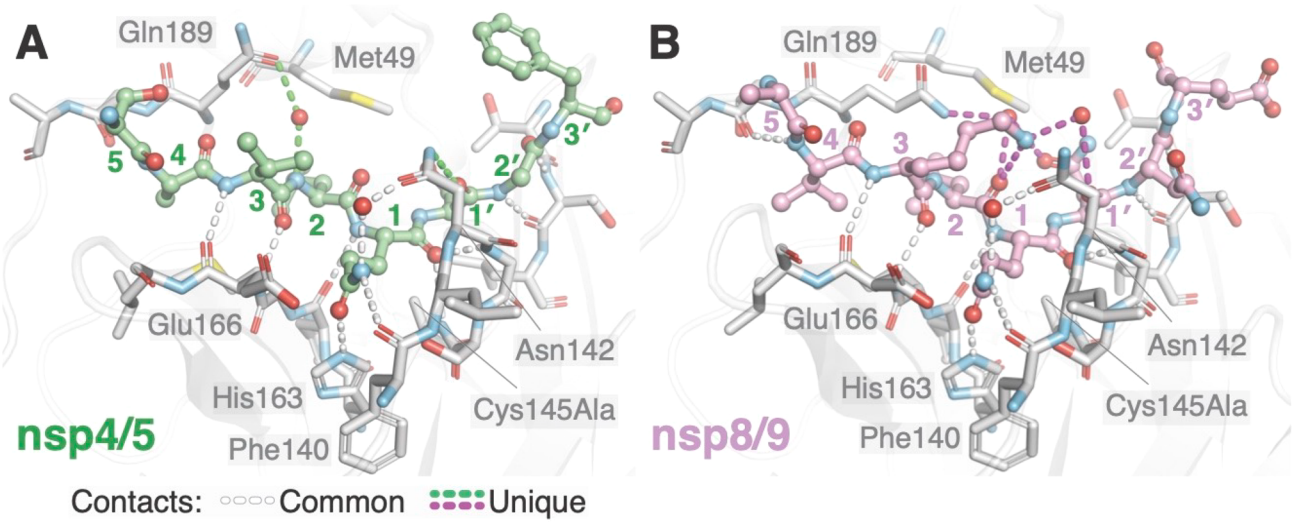

Figure 2. Differential recognition of nsp4/5 and nsp8/9 substrates by M^{pro}. Identical views of nsp4/5 (A) and nsp8/9 (B) substrates in the M^{pro}Cys145Ala active site. Substrate peptide P and P′ residues are labeled with colored numbers. Key M^{pro} residues mentioned in the text are labeled. Conserved hydrogen bonds enabling M^{pro} recognition of substrate mainchain and P1 Gln side chain atoms are shown as white dashed lines. Hydrogen bonds that differ between the complex with nsp4/5 and that with nsp8/9 are shown in green and magenta, respectively. M^{pro} Asn142 and Gln189 contact both substrates through bound water molecules, and the resulting networks of hydrogen bonds differ between the two substrates.

nsp12. We have used X-ray crystallography to study nsp8/9 and nsp4/5 recognition by M^{pro}. The structures show unique features of the M^{pro}·nsp8/9 complex and highlight the importance of P1′−P3′ residues in catalysis.

To study M^{pro} activity, we monitored the cleavage of labeled substrate peptides *in vitro* and derived Michaelis−Menten parameters describing the reactions. M^{pro} cleavage of nsp4/5 is more efficient than cleavage of nsp8/9 (36-fold difference in k_{cat}/K_M; Table 1, Figure S1).[13] We sought to understand the influence of the Asn residues at the P1′ and P2′ sites of the nsp8/9 substrate (Table 1). Alteration of the steric properties by alanine substitution at either position approximately doubled the catalytic efficiency. The P1′ Asn-to-Ala substitution lowered K_M and raised k_{cat}, while P2′ substitution only raised k_{cat}. Installation of an isosteric Asp residue at the P1′ position completely abrogated activity, while the analogous Asn-to-Asp substitution at P2′ diminished but did not abrogate activity. We suspect that placing additional negative charge near the active site raises the energetic barrier to attaining the oxyanion transition states.[14,15]

Differences in k_{cat} for the tested substrates dominated the small changes in K_M and drove the observed changes in k_{cat}/K_M. The P5−P1 residues were constant for nsp8/9 and its derivatives, ruling out acyl-enzyme hydrolysis as the step that determines k_{cat}. Therefore, either formation of the enzyme−substrate complex or conversion to the acyl-enzyme intermediate must limit k_{cat} for the nsp8/9 substrate, and similar K_M values imply the latter is true. These data imply kinetic competition among the 11 viral M^{pro} substrates during virus replication.

To better understand the different cleavage efficiencies, we determined crystal structures of M^{pro} bound to the nsp4/5 and nsp8/9 substrates (Figure 2). The structures were resolved to 1.84 Å for nsp4/5 and 1.94 Å for nsp8/9 (Table S1), which enabled a detailed interpretation of the atomic contacts between the enzyme and both substrates. The active site Cys145Ala mutation trapped the intact substrates and enabled visualization of the P′ residues (Figure S2). The C145A mutation creates a cavity in the M^{pro} active site that could influence the position of the scissile bond. At least one previous study has used the M^{pro} H41A mutation to circumvent this potential problem.[16] Nevertheless, the high resolutions of both structures, the unambiguous positions of both scissile bonds, and the apparent specificity of peptide−enzyme contacts permitted a detailed analysis of substrate engagement in both cases.

Eleven conserved hydrogen bonds occur between M^{pro} and each of the substrates (Figure 2, white dashed lines). Eight contacts between the peptide backbones of enzyme and substrate are shared among SARS-CoV nsp4/5, PEDV nsp4/5,[16,17] and the two severe acute respiratory syndrome coronavirus 2 (SARS-CoV-2) peptides reported here. M^{pro}

https://doi.org/10.1021/acsinfecdis.1c00237
ACS Infect. Dis. XXXX, XXX, XXX−XXX

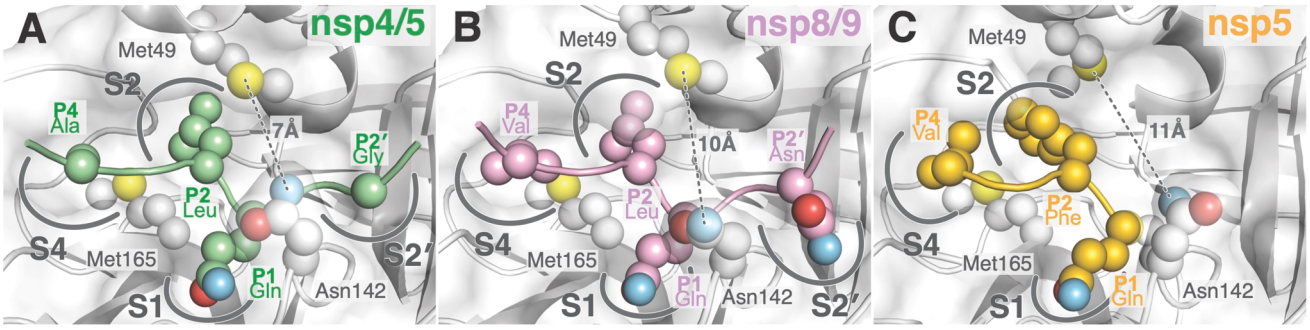

Figure 3. Steric effects that influence substrate recognition and M^{pro} activity. Spheres show positions of atoms dictating shape complementarity between M^{pro} subsites and nsp4/5 (A), nsp8/9 (B), and nsp5 (C; acyl-enzyme intermediate, PDB 7KHP). Labels show M^{pro} subsites and the distance between M^{pro} Met49 and Asn142 (thioether to amide nitrogen).

Gly143 and Ala145 mainchain amides form the oxyanion hole by donating a pair of hydrogen bonds to the scissile P1 carbonyl oxygen, which stabilizes the developing negative charge during covalent catalysis. His163 and the mainchain carbonyl of Phe140 make hydrogen bonds with the invariant side chain of the P1 Gln, and Asn142 contacts the P1 Gln through a conserved water bridge. Neither SARS-CoV nor PEDV M^{pro}·nsp4/5 complexes show the hydrogen bonds observed with Asn142 in the SARS-CoV2 substrate complexes.[16,17]

Substrate interactions with the M^{pro} Asn142 and Gln189 side chains distinguish nsp4/5 and nsp8/9 recognition (Figure 2, green and magenta dashed lines). M^{pro} Asn142 forms a hydrogen bond with the nsp4/5 P1′ backbone carbonyl oxygen, and M^{pro} Gln189 forms a water bridge with the nsp4/5 P2 amide nitrogen. In contrast, M^{pro} Gln189 engages the nsp8/9 P3 and P1′ side chains via an ordered water molecule. In addition to these contacts, the ordered waters found in the nsp8/9-bound structure could donate hydrogen bonds to the P1′ and P2 mainchain carbonyl oxygens. Finally, the nsp8/9 P3 Lys forms a hydrogen bond with the P2 carbonyl.

The peptide recognition described above supports distinct modes of P′ fragment accommodation by M^{pro} for the nsp4/5 and nsp8/9 substrates. The near-invariant nsp8/9 P1′ and P2′ Asn side chains are bulkier than the P1′ (Ser/Ala) and P2′ (Gly/Ala) side chains of other M^{pro} substrates, although there is greater tolerance for P2′ diversity.[18] The nsp8/9 P1′ Asn projects more deeply into the S1′ subsite than the nsp4/5 P1′ Ser and therefore likely restrains the P′ peptide to a greater degree. M^{pro} Asn142 and Gly143 coordinate the nsp8/9 P2′ residue through peptide backbone interactions, and similar interactions position the nsp4/5 P2′ Gly. Overall, the bulkier nsp8/9 Asn side chains in the S1′ and S2′ subsites shift nsp8/9 relative to nsp4/5 (Figure 3A,B), and the resulting alignment with the M^{pro} cysteine nucleophile differs slightly (Figure S3). In addition to this small change in the position of the scissile bond, the nsp8/9 substrate bends away from the enzyme, resulting in an ∼1.5 Å displacement of P4 and P4′ C^{α} positions relative to nsp4/5 (Figure S3) and widening the active site cleft formed between M^{pro} Met49 and Asn142 (7 to 10 Å, Figure 3A,B). These differences provide an explanation for reduced catalytic efficiency for the nsp8/9 substrate. The alanine substitutions discussed above presumably restore catalytic efficiency by enabling nsp8/9 to adopt an overall conformation and position more like nsp4/5.

Hydrophobic interactions dictate the recognition of N-terminal substrate fragments (P residues, excluding the invariant P1 Gln). M^{pro} Met49 and Met165 define the S2 subsite (Figure 3). The nsp4/5 P4 Ala is smaller than the ns8/9 P3 Val, allowing nsp4/5 to sit more deeply in the S4 subsite (Figure 3A,B). A recent crystal structure shows that the intact nsp5/6 substrate is also shifted relative to nsp4/5 due to a bulky Phe at the P2 position (Figure 3C).[8] Indeed, M^{pro} cleavage is most efficient for peptides bearing P2 Leu and less efficient for those bearing P2 Phe.[19] Like nsp8/9, cleavage of SARS nsp5/6 depends more heavily on P′ recognition than nsp4/5 does.[20,21]

The nsp8/9 P3 Lys might also limit catalysis. Water bridges connect their terminal nitrogen (N^{ζ}) with the nsp8/9 P1′ Asn (mentioned above), and the resulting conformation could slow peptide accommodation to the M^{pro} active site. Therefore, diverse M^{pro}−substrate interactions contribute to finely tuned substrate geometry that results in substrate-specific catalytic efficiency.[22]

The structures we have determined show how M^{pro} active site plasticity and substrate evolution can tune catalysis. Slow cleavage of the nsp8/9 junction, which is observed among disparate coronaviruses, might be a selected trait required for the coordinated assembly of the RNA replication machinery.[9,13,23,24] Distinct kinetic parameters associated with cleavage of the viral substrate could be important for maturation of the viral polyprotein. The need for the nsp8/9 junction to support both M^{pro} cleavage and nsp12 binding (and subsequent nucleotide monophosphate acceptance) accounts for the near-invariance of the P1−P2′ residues. The sequence is therefore a compromise that satisfies the requirements of two unrelated catalytic mechanisms, and mimicry of the nsp8/9 junction presents a unique opportunity to chemically inhibit both M^{pro} and the viral polymerase.

The structures also present templates for new protease inhibitor scaffolds. In particular, the nsp8/9 P3 side chain can fold back to contact P1′, suggesting macrocyclic inhibitors could mimic this interaction. Similar strategies have been pursued for Hepatitis C NS3, HIV-1, and Rhinovirus 3C proteases.[25−27] Kinetic analyses of nsp8/9 and its variants suggests that inhibitor P1′ and P2′ site contacts could influence the formation of covalent inhibitor−enzyme adducts. While α-ketoamide warheads have been investigated as ligands for M^{pro} Cys145,[3] more comprehensive exploration of this warhead in combination with P′ mimicry could be beneficial.

METHODS

Complete methods are included in the Supporting Information associated with this report. A plasmid for recombinant

https://doi.org/10.1021/acsinfecdis.1c00237
ACS Infect. Dis. XXXX, XXX, XXX−XXX

expression of codon-optimized SARS-CoV-2 main protease (M^{pro}) was a gift from Zhang et al.[3] M^{pro} expressed and purified from *E. coli* carrying this plasmid was used for peptide cleavage assays. M^{pro} Cys145Ala was purified from *E. coli* as a SUMO fusion protein. The N-terminus was generated by Ulp1 cleavage before use in crystallography experiments.

For crystallization, M^{pro} Cys145Ala was incubated with a 10-fold molar excess of each peptide (nsp4/5, AVLQSGFRK; nsp8/9, AVKLQNNEL) before mixing with the mother liquor. Crystallization conditions are given in the Supporting Information. Diffraction data were collected at the Advanced Photon Source on NE-CAT beamline 24-IDC.

Enzyme kinetics were determined using Förster resonance energy transfer (FRET) substrate peptides labeled with N-terminal fluorophore Dabcyl and C-terminal quencher Edans. Increasing concentrations of labeled substrates were incubated with Mpro (0.25 μM for nsp4/5 experiments and 0.4 μM for nsp8/9 experiments), and fluorescence was measured. Absolute product concentrations were determined and used to convert initial velocities to nM/s for triplicate reactions at each substrate concentration. Michaelis–Menten parameters (K_M and k_{cat}) were determined using Prism 6 software.

■ ASSOCIATED CONTENT

Supporting Information

The Supporting Information is available free of charge at https://pubs.acs.org/doi/10.1021/acsinfecdis.1c00237.

Methods, inhibition experiments, and crystallographic information (PDF)

Accession Codes

Crystallographic data have been deposited at the PDB with associated codes 7MGR (M^{pro}·nsp8/9) and 7MGS (M^{pro}·nsp4/5).

■ AUTHOR INFORMATION

Corresponding Authors

Stephen M. Hinshaw − *Department of Biological Chemistry and Molecular Pharmacology, Harvard Medical School, Boston, Massachusetts 02115, United States;* Present Address: S.M.H.: Stanford Cancer Institute, Stanford University School of Medicine, Stanford, CA, USA; orcid.org/0000-0003-4215-5206; Email: hinshaw@crystal.harvard.edu

Ian W. Windsor − *Laboratory of Molecular Medicine, Boston Children's Hospital, Boston, Massachusetts 02115, United States; Department of Biological Chemistry and Molecular Pharmacology, Harvard Medical School, Boston, Massachusetts 02115, United States; Ragon Institute of MGH, MIT, and Harvard, Cambridge, Massachusetts 02139, United States;* orcid.org/0000-0002-6289-6928; Email: windsor@crystal.harvard.edu

Authors

Elizabeth A. MacDonald − *Laboratory of Molecular Medicine, Boston Children's Hospital, Boston, Massachusetts 02115, United States*

Gary Frey − *Department of Pediatrics and ICCB-Longwood Screening Facility, Harvard Medical School, Boston, Massachusetts 02115, United States*

Mark N. Namchuk − *Department of Biological Chemistry and Molecular Pharmacology, Harvard Medical School, Boston, Massachusetts 02115, United States;* orcid.org/0000-0002-5220-2275

Stephen C. Harrison − *Laboratory of Molecular Medicine, Boston Children's Hospital, Boston, Massachusetts 02115, United States; Department of Biological Chemistry and Molecular Pharmacology, Harvard Medical School, Boston, Massachusetts 02115, United States; Howard Hughes Medical Institute, Boston, Massachusetts 02115, United States*

Complete contact information is available at: https://pubs.acs.org/10.1021/acsinfecdis.1c00237

Notes

The authors declare the following competing financial interest(s): M.N.N. is the recipient of funding from Abbvie. The funding did not contribute to this work.

■ ACKNOWLEDGMENTS

We acknowledge funding support from the Massachusetts Consortium for Pathogen Readiness (M.N.N.), the Howard Hughes Medical Institute (S.C.H.), and the Nancy Lurie Marks Family Foundation (S.C.H.). S.M.H. is an HHMI Fellow of the Helen Hay Whitney Foundation. NE-CAT is funded by NIH grant P30 GM 124165. Advanced Photon Source (APS) is operated for the DOE Office of Science by Argonne National Laboratory under contract DE-AC02-06CH11357. Enzyme assays were performed at the Institute for Chemistry and Chemical Biology (ICCB-Longwood) at Harvard Medical School. We thank Linlin Zhang (Hilgenfeld Laboratory, University of Lübeck) for providing the codon-optimized Mpro expression plasmid. X-ray diffraction data were collected at the APS on NE-CAT beamline 24-IDC.

■ REFERENCES

(1) Anand, K.; Ziebuhr, J.; Wadhwani, P.; Mesters, J. R.; Hilgenfeld, R. Coronavirus main proteinase (3CLpro) structure: basis for design of anti-SARS drugs. *Science* **2003**, *300*, 1763−1767.

(2) Hilgenfeld, R. From SARS to MERS: crystallographic studies on coronaviral proteases enable antiviral drug design. *FEBS J.* **2014**, *281*, 4085−4096.

(3) Zhang, L.; Lin, D.; Sun, X.; Curth, U.; Drosten, C.; Sauerhering, L.; Becker, S.; Rox, K.; Hilgenfeld, R. Crystal structure of SARS-CoV-2 main protease provides a basis for design of improved alpha-ketoamide inhibitors. *Science* **2020**, *368*, 409−412.

(4) Lockbaum, G. J.; Reyes, A. C.; Lee, J. M.; Tilvawala, R.; Nalivaika, E. A.; Ali, A.; Kurt Yilmaz, N.; Thompson, P. R.; Schiffer, C. A. Crystal Structure of SARS-CoV-2 Main Protease in Complex with the Non-Covalent Inhibitor ML188. *Viruses* **2021**, *13*, 174.

(5) Ma, C.; Sacco, M. D.; Hurst, B.; Townsend, J. A.; Hu, Y.; Szeto, T.; Zhang, X.; Tarbet, B.; Marty, M. T.; Chen, Y.; Wang, J. Boceprevir, GC-376, and calpain inhibitors II, XII inhibit SARS-CoV-2 viral replication by targeting the viral main protease. *Cell Res.* **2020**, *30*, 678−692.

(6) Rathnayake, A. D.; Zheng, J.; Kim, Y.; Perera, K. D.; Mackin, S.; Meyerholz, D. K.; Kashipathy, M. M.; Battaile, K. P.; Lovell, S.; Perlman, S.; Groutas, W. C.; Chang, K. O. 3C-like protease inhibitors block coronavirus replication in vitro and improve survival in MERS-CoV-infected mice. *Sci. Transl. Med.* **2020**, *12*, eabc5332.

(7) Dai, W.; Zhang, B.; Jiang, X. M.; Su, H.; Li, J.; Zhao, Y.; Xie, X.; Jin, Z.; Peng, J.; Liu, F.; Li, C.; Li, Y.; Bai, F.; Wang, H.; Cheng, X.; Cen, X.; Hu, S.; Yang, X.; Wang, J.; Liu, X.; Xiao, G.; Jiang, H.; Rao, Z.; Zhang, L. K.; Xu, Y.; Yang, H.; Liu, H. Structure-based design of antiviral drug candidates targeting the SARS-CoV-2 main protease. *Science* **2020**, *368*, 1331−1335.

(8) Lee, J.; Worrall, L. J.; Vuckovic, M.; Rosell, F. I.; Gentile, F.; Ton, A. T.; Caveney, N. A.; Ban, F.; Cherkasov, A.; Paetzel, M.; Strynadka, N. C. J. Crystallographic structure of wild-type SARS-CoV-2 main protease acyl-enzyme intermediate with physiological C-terminal autoprocessing site. *Nat. Commun.* **2020**, *11*, 5877.
(9) Hegyi, A.; Ziebuhr, J. Conservation of substrate specificities among coronavirus main proteases. *J. Gen. Virol.* **2002**, *83*, 595−599.
(10) Deming, D. J.; Graham, R. L.; Denison, M. R.; Baric, R. S. Processing of open reading frame 1a replicase proteins nsp7 to nsp10 in murine hepatitis virus strain A59 replication. *J. Virol.* **2007**, *81*, 10280−10291.
(11) Yan, L.; Ge, J.; Zheng, L.; Zhang, Y.; Gao, Y.; Wang, T.; Huang, Y.; Yang, Y.; Gao, S.; Li, M.; Liu, Z.; Wang, H.; Li, Y.; Chen, Y.; Guddat, L. W.; Wang, Q.; Rao, Z.; Lou, Z. Cryo-EM Structure of an Extended SARS-CoV-2 Replication and Transcription Complex Reveals an Intermediate State in Cap Synthesis. *Cell* **2021**, *184*, 184−193.E10.
(12) Slanina, H.; Madhugiri, R.; Bylapudi, G.; Schultheiss, K.; Karl, N.; Gulyaeva, A.; Gorbalenya, A. E.; Linne, U.; Ziebuhr, J. Coronavirus replication-transcription complex: Vital and selective NMPylation of a conserved site in nsp9 by the NiRAN-RdRp subunit. *Proc. Natl. Acad. Sci. U. S. A.* **2021**, *118*, e2022310118.
(13) Krichel, B.; Falke, S.; Hilgenfeld, R.; Redecke, L.; Uetrecht, C. Processing of the SARS-CoV pp1a/ab nsp7−10 region. *Biochem. J.* **2020**, *477*, 1009−1019.
(14) Robertus, J. D.; Kraut, J.; Alden, R. A.; Birktoft, J. J. Subtilisin; a stereochemical mechanism involving transition-state stabilization. *Biochemistry* **1972**, *11*, 4293−4303.
(15) Simon, L.; Goodman, J. M. Enzyme catalysis by hydrogen bonds: the balance between transition state binding and substrate binding in oxyanion holes. *J. Org. Chem.* **2010**, *75*, 1831−1840.
(16) Xue, X.; Yu, H.; Yang, H.; Xue, F.; Wu, Z.; Shen, W.; Li, J.; Zhou, Z.; Ding, Y.; Zhao, Q.; Zhang, X. C.; Liao, M.; Bartlam, M.; Rao, Z. Structures of two coronavirus main proteases: implications for substrate binding and antiviral drug design. *J. Virol.* **2008**, *82*, 2515−2527.
(17) Ye, G.; Deng, F.; Shen, Z.; Luo, R.; Zhao, L.; Xiao, S.; Fu, Z. F.; Peng, G. Structural basis for the dimerization and substrate recognition specificity of porcine epidemic diarrhea virus 3C-like protease. *Virology* **2016**, *494*, 225−235.
(18) Koudelka, T.; Boger, J.; Henkel, A.; Schonherr, R.; Krantz, S.; Fuchs, S.; Rodriguez, E.; Redecke, L.; Tholey, A. N-Terminomics for the Identification of In Vitro Substrates and Cleavage Site Specificity of the SARS-CoV-2 Main Protease. *Proteomics* **2021**, *21*, 2000246.
(19) Rut, W.; Groborz, K.; Zhang, L.; Sun, X.; Zmudzinski, M.; Pawlik, B.; Wang, X.; Jochmans, D.; Neyts, J.; Mlynarski, W.; Hilgenfeld, R.; Drag, M. SARS-CoV-2 M(pro) inhibitors and activity-based probes for patient-sample imaging. *Nat. Chem. Biol.* **2021**, *17*, 222−228.
(20) Muramatsu, T.; Takemoto, C.; Kim, Y. T.; Wang, H.; Nishii, W.; Terada, T.; Shirouzu, M.; Yokoyama, S. SARS-CoV 3CL protease cleaves its C-terminal autoprocessing site by novel subsite cooperativity. *Proc. Natl. Acad. Sci. U. S. A.* **2016**, *113*, 12997−13002.
(21) Xue, X.; Yang, H.; Shen, W.; Zhao, Q.; Li, J.; Yang, K.; Chen, C.; Jin, Y.; Bartlam, M.; Rao, Z. Production of authentic SARS-CoV M(pro) with enhanced activity: application as a novel tag-cleavage endopeptidase for protein overproduction. *J. Mol. Biol.* **2007**, *366*, 965−975.
(22) Kneller, D. W.; Phillips, G.; O'Neill, H. M.; Jedrzejczak, R.; Stols, L.; Langan, P.; Joachimiak, A.; Coates, L.; Kovalevsky, A. Structural plasticity of SARS-CoV-2 3CL M(pro) active site cavity revealed by room temperature X-ray crystallography. *Nat. Commun.* **2020**, *11*, 3202.
(23) Gildenhuys, S. Expanding our understanding of the role polyprotein conformation plays in the coronavirus life cycle. *Biochem. J.* **2020**, *477*, 1479−1482.
(24) Snijder, E. J.; Decroly, E.; Ziebuhr, J. The Nonstructural Proteins Directing Coronavirus RNA Synthesis and Processing. *Adv. Virus Res.* **2016**, *96*, 59−126.
(25) Li, X.; Zhang, Y. K.; Liu, Y.; Ding, C. Z.; Zhou, Y.; Li, Q.; Plattner, J. J.; Baker, S. J.; Zhang, S.; Kazmierski, W. M.; Wright, L. L.; Smith, G. K.; Grimes, R. M.; Crosby, R. M.; Creech, K. L.; Carballo, L. H.; Slater, M. J.; Jarvest, R. L.; Thommes, P.; Hubbard, J. A.; Convery, M. A.; Nassau, P. M.; McDowell, W.; Skarzynski, T. J.; Qian, X.; Fan, D.; Liao, L.; Ni, Z. J.; Pennicott, L. E.; Zou, W.; Wright, J. Novel macrocyclic HCV NS3 protease inhibitors derived from alpha-amino cyclic boronates. *Bioorg. Med. Chem. Lett.* **2010**, *20*, 5695−5700.
(26) Ghosh, A. K.; Sean Fyvie, W.; Brindisi, M.; Steffey, M.; Agniswamy, J.; Wang, Y. F.; Aoki, M.; Amano, M.; Weber, I. T.; Mitsuya, H. Design, synthesis, X-ray studies, and biological evaluation of novel macrocyclic HIV-1 protease inhibitors involving the P1′-P2′ ligands. *Bioorg. Med. Chem. Lett.* **2017**, *27*, 4925−4931.
(27) Namoto, K.; Sirockin, F.; Sellner, H.; Wiesmann, C.; Villard, F.; Moreau, R. J.; Valeur, E.; Paulding, S. C.; Schleeger, S.; Schipp, K.; Loup, J.; Andrews, L.; Swale, R.; Robinson, M.; Farady, C. J. Structure-based design and synthesis of macrocyclic human rhinovirus 3C protease inhibitors. *Bioorg. Med. Chem. Lett.* **2018**, *28*, 906−909.

https://doi.org/10.1021/acsinfecdis.1c00237
ACS Infect. Dis. XXXX, XXX, XXX−XXX